Spreadability of Metal Powders for Laser-Powder Bed Fusion via Simple Image Processing Steps

Cekdar Vakifahmetoglu[1, *], Beyza Hasdemir[1,2]

[1]Department of Materials Science and Engineering, Izmir Institute of Technology, Urla, Izmir, Turkey.

[2]Sentes-BIR, R&D Center, Izmir, Turkey.

E-mail: cekdarvakifahmetoglu@iyte.edu.tr or cvahmetoglu@gmail.com

Abstract

This paper investigates the spreadability of the spherical CoCrWMo powder for Laser-Powder Bed Fusion (PBF-LB) by using image processing algorithms coded in MATLAB. Besides, it also aims to examine the spreadability correlation with the other characteristics such as flow rate, apparent density, angle of repose. Powder blends in four different particle size distributions_are prepared, characterized, and spreadability tests are performed with the PBF-LB. The results demonstrate that an increase in fine particle ratio by volume (below 10 µm) enhances the agglomeration and decreases the flowability, causing poor spreadability. These irregularities on the spread layers are quantified with simple illumination invariant analysis.

Keywords: additive manufacturing, spreadability, powder bed fusion, gas atomization, illumination invariant

1. Introduction

Powder Bed Fusion (PBF) is an Additive Manufacturing (AM) technique wherein spread powder layers were consolidated by a heat source to obtain three-dimensional (3D) components. According to the F42 Committee based on AM in American Society for Testing Materials (ASTM), AM methods are categorized into seven areas: Material Extrusion (MEX), Vat Photopolymerization (VP), Material Jetting (MJ), Sheet Lamination (SL), Powder Bed Fusion (PBF), Binder Jetting (BJ) and Directed Energy Deposition (DED) [1, 2]. Among all; PBF, BJ, MJ, and DED currently use spherical metal powders as a feedstock to obtain

metallic components. For PBF processes [1, 3-8], the powder homogeneity is important since a smooth layer may provide decent properties. Homogeneity on the powder bed layer depends on powder properties such as size, cohesion, impurities, apparent/tapped density, moisture, shape, roughness, etc [9, 10].

Standard characterization methods of powder metallurgy cannot unfortunately adequately meet the expected properties for AM. In 2014, the ASTM F42 committee created ASTM F3049 for the characterization of metal powders for AM. Specific powder properties marked are particle size distribution, particle morphology, chemical composition, true density, and impurity content (C, S, O, N, H, etc.). Bulk powder properties are categorized as flow rate, apparent density, tap density, and angle of repose [11]. In this context, the purpose of DIN EN ISO / ASTM 52907 is to simplify customer and supplied relation to acquire metallic powder for AM [12].

In the past decade, a considerable amount of research has been conducted towards the investigation of powder characteristics for AM. Particularly for metal powders used in PBF, a very recent study investigated the effect of spreading velocity, layer thickness, and powder morphology on layer uniformity. In brief, it was shown that texture and sphericity were important to define the spreader velocity which was critically important for the uniformity of the powder [13]. Other studies focused on the role of particle-related properties (particle size distribution, morphology, flowability, etc.) on the processability of the Ti6Al4V, 316L, and AlSi10Mg alloys [14, 15]. It was shown that, when fine particles (D_{50} = 9 µm) were used because of lower flowability, the components with lower dimensional accuracy were obtained compared to coarse ones (D_{50} = 40 µm) [15]. Besides, spread characteristics and powder bed packing density were shown to be affected by shape irregularities and particle roughness of the 316L. Bad spreadability can cause inhomogeneity and affect the regularity of the powder bed surface [16]. Additionally, the angle of repose (AOR) is related in many studies to the powder flowability with a brief outcome that is the smaller the AOR the better the flowability [14, 17, 18]. In a different work [19], studied the effect of recycling on the 304 L stainless steel powder for the PBF process. Flowability of the recycled powder was improved due to (i) a decrease in the number of fines, (ii) more spherical, and (iii) surface oxide formation reducing the friction and surface energy at the interparticle contacts lessening adhesion. Similarly, in a recent review on the recycling of metal powders in AM, the importance of flowability on the final component produced by the PBF method was examined [20]. However, still in practical applications, the suitability of the powder layer for PBF is

determined by the observation of an operator or by in situ cameras in the 3D printing machine [21].

It is not an easy task to form a spread layer with a homogeneous powder distribution which is crucial to fulfill the demanded final properties. Spreadability can be defined as a way to quantify the powder distribution through the layer. Currently, there is no standardized characterization method for spreadability for the metal powder layer, and it is currently controlled merely by following the powder flowability, which is the result of the combination of physical properties affecting the flow behavior [22]. In addition to that, there are very limited published works in regard; e.g., In 2019, researchers proposed that powder spreadability among all metrics can be determined by the build plate coverage ratio, the rate of powder deposition, and the alteration rate of the avalanche angle in powder-bed systems [18]. In a more recent study [23], it was shown that particle morphology and size distribution was important for a homogenous spread layer and better mechanical properties of the 3D printed component. Similarly, flowability and apparent density were directly affected by the PSD, surface topology, and morphology of the powder in PBF-LB applications [10]. Moreover, spreading dynamics were investigated by high-speed high-energy x-ray imaging, and it was shown that the average powder size is an important parameter affecting the flow during spreading [24].

Few modeling studies have also been conducted to analyze powder spreadability, e.g., [25] have used the Discrete Element Method (DEM) simulation at the particle level to determine the packing density of the powder layer for the powder-spreading process. The authors concluded that the packing density of powders with a higher portion of fine particles is low due to the agglomeration, i.e. high cohesive forces. The utilization of bimodal (fine and coarse), powder mixtures was not successful as well due possibly to the segregation and voids in the layer. While few studies did similar simulations for powder spreadability characterization as well [26-28] but no other studies have so far been found to propose a simple technique. Such scarce data is in fact due partially to 3D printer manufacturers since they market their instruments with already defined production parameters and raw metal powder sources (same for polymeric and ceramic materials). The companies impose the utilization of such defined parameters and powder sources to guarantee, and otherwise, they do not provide any assurance of the produced parts.

The aim of this study is to add knowledge and develop a simple illumination invariant method by investigating the powder characteristics using digital photos acquired by a simple cell-phone camera and applying an image processing algorithm in MATLAB. Besides, it will be

correlated with other existing characterization methods such as flow rate, apparent density, angle of repose of a model CoCrMoW metallic powder which is commonly used in dental applications such as dental crowns and bridges, for PBF-LB. This research may also open new avenues to provide information on the utilization of outsourced powders that can be used in any available machine, a step further study to render a general tool that is applicable in PBF processes.

2. Experimental Procedure

Spherical CoCrWMo powder (PURESPHERE 43055; Mn:0.08 wt.%, Cr:26.82 wt.%, Mo:4.66 wt.%, W:5.40 wt.%, Si:0.90 wt.%, kindly supplied by Sentes-BIR A.S., Izmir, Turkey) produced by gas atomization was used as is in all experiments. Four different powder mixtures coded as M15-45, Mix1, Mix2, and Mix3 were prepared by sieving according to specified particle sizes. Retsch Sieve Shaker (AS200 Basic, Germany) with 20 µm, 38 µm, 45 µm, and 63 µm sieves were used. According to visual examinations, M15-45, Mix2, and Mix3 were more flowable, while Mix1 were non-flowable due probably to the higher portion of agglomerates.

PBF-LB (Laseral MTL90 with Yt-fiber: 200 W and wavelength of 1064 nm, Izmir, Turkey) machine, was used for spreadability tests, chamber environment was kept under pure N_2 (> %99.9 pure) to ensure the oxygen content was limited to 0.1 wt.%. For spreadability tests which always done at a constant spreading speed (200 mm s^{-1}) with a continuous layer thickness of 50 µm, the printer spreading system was modified to install a Bluetooth controlled cell phone fixed with stainless steel apparatus having a 6 mm diameter aperture for the digital camera (8-megapixel, f/2.2, 1.5 µm) of the cell phone (iPhone 6). A rubber blade on a 30 mm diameter building platform with white LEDs bonded to black cardboard was used.

To characterize the spreadability behavior, preliminary studies were done with the samples having deliberately made irregularities.

The camera images of the spreads were processed by Wiener filtering in MATLAB, (see **Figure 1(a-f)**). Initially, edge detection (`*canny*`) operation was applied to detect the boundary of the circular region. Then, after finding the center and the radius of the boundary circle using the circular Hough transform, thresholding (*Otsu* method) was conducted inside the extracted circle to calculate black to white ratio simply from the number of black and white pixels, and further average grayscale value in between 0 to 255. It should be noted that here only average grayscale values are given, however, the standard deviation of grayscale

values may be useful to properly demonstrate the homogeneity for which further dedicated studies are needed.

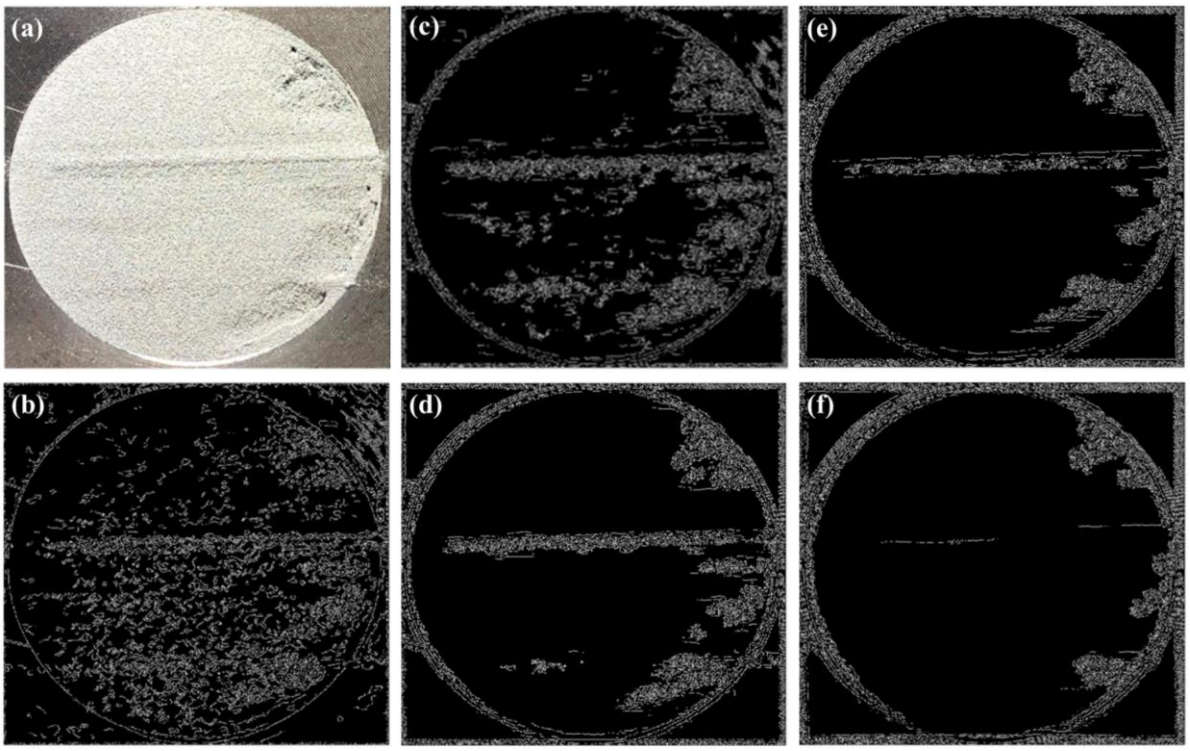

Figure 1. Obtained images for a model poor spread layer (a) without any operation, and upon 2D Wiener noise removal filtering with different neighborhood sizes; (b) 10, (c) 20, (d) 30, (e) 40, and (f) 50.

The morphological characterizations were done by Scanning Electron Microscopy (SEM; Thermo Scientific Apreo S, MA, USA). The particle size was measured both by Laser Diffraction Analyzer (Malvern Panalytical Mastersizer 2000, UK) and by using the SEM images with the ImageJ software (ImageJ 1.52a, National Institutes of Health, USA) to quantify the average data (from 100 measurements). Flow rate, apparent density, and angle of repose measurements were conducted by Hall flowmeter (produced according to ASTM B212 standard by Sentes-BIR, Izmir, Turkey). Tapped density measurement was performed by Tapped Density instrument (produced according to ASTM B527 standard by Sentes-BIR, Izmir, Turkey). The chemical composition of the used powder was measured by Inductively Coupled Plasma Emission Spectroscopy (Perkin Elmer Avio 200, MA, USA). The oxygen amount was measured with an inert gas fusion principle (Leco TC400, LECO, MI, USA).

3. Results & Discussion

3.1. CoCrWMo Characteristics

The characteristics of the CoCrWMo powder mixtures, coded as M15-45, Mix1, Mix2, and Mix3 analyzed by laser diffraction. While D_{10}, D_{50}, and D_{90} values of the M15-45 and Mix2 were similar to each other, M15-45 was used since it is a generally recommended powder distribution type for AM, and still there were slight differences in the amount of the particles below 20 µm and above 45 µm. Mix1 had a high ratio of particles below 20 µm being 66.58 %, and instead, Mix3 included coarser particles higher in volume.

The particle size distribution (PSD) plots obtained from both laser diffraction and microscopic evaluations (SEM) are given in **Figure 2(a) and Figure 2(b),** respectively**.** For the morphological investigation, the stereological equation $D_{sphere} = D_{circle}/0.785$ was applied to convert 2D measurements to 3D values [29, 30]. The average particle size was assessed as; 31.27 ± 9.46 µm for M15-45, 18.54 ± 7.05, µm for Mix1, 34.30 ± 6.97 µm for Mix2, and 58.72 ± 7.08 µm for Mix3, comparable with the laser diffraction obtained D50 values, as seen also in other works [31].

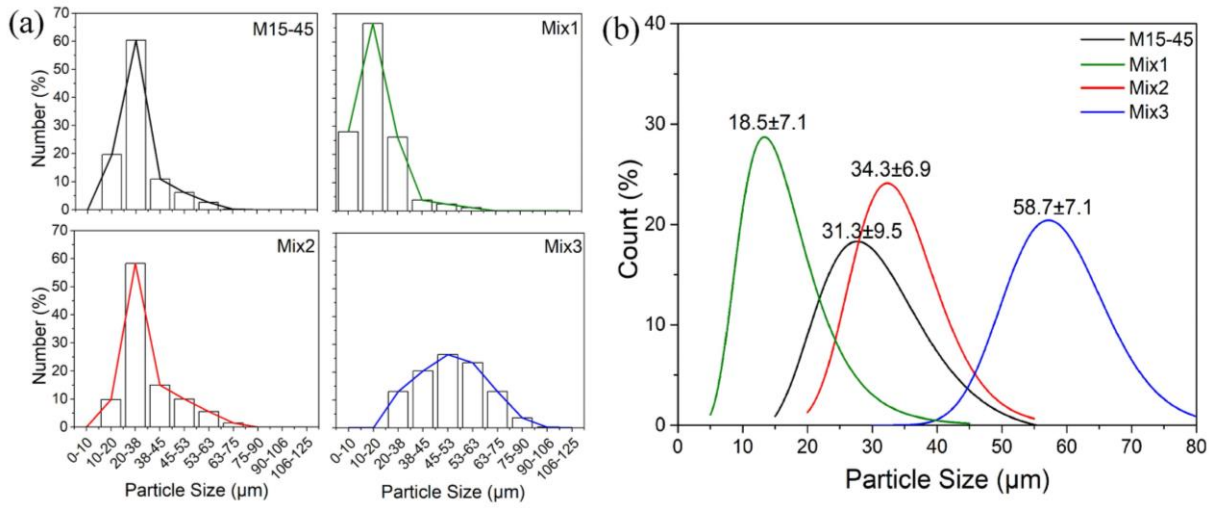

Figure 2. The particle size distribution (PSD) plots of the samples obtained from; (a) laser diffraction, and (b) SEM image analysis from 100 measurements.

The morphologies of the powder mixtures principally being spherical were shown in **Figure 3**. Few non-spherical particles, i.e., irregularities, can be explained with gas atomization process parameters. As known for example the powder morphology is directly related to the cooling rate during atomization that is affected by melting temperature of the metal or alloy, atomization pressure, free-fall distance, and gas to metal ratio.

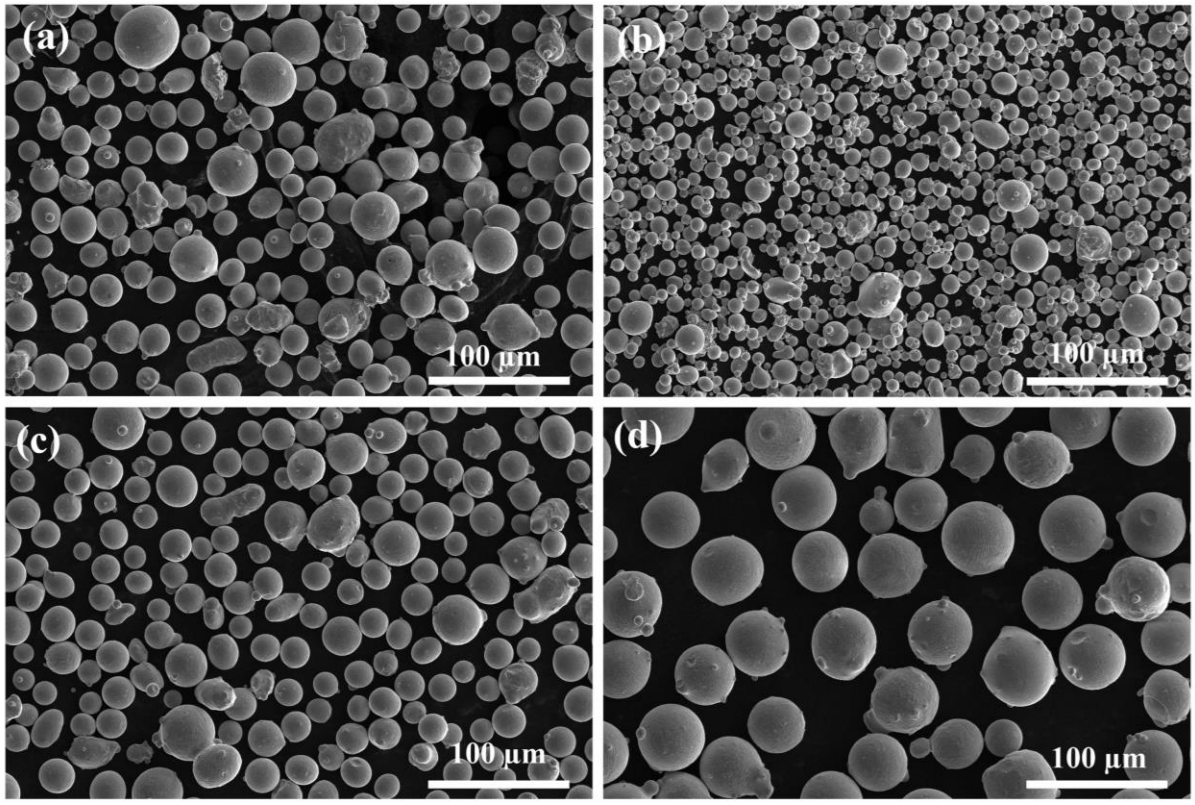

Figure 3. SEM images of CoCrWMo powder blends in different particle size distribution; (a) M15-45, (b) Mix1, (c) Mix2, and (d) Mix3.

The angle of repose (AOR, α) is related to where *H* is the height, *D* is the diameter of the formed powder triangle as given in (Equation 1):

$$\alpha = \tan^{-1}\left(\frac{2H}{D}\right) \quad (1)$$

Figure 4 shows the AOR measurements of Mix1 and Mix3. The latter was a quite cohesive powder due to the higher fine particle ratio (particles below 20 µm was 66.58 vol%) and was measured as 32.85º. Instead, Mix3 was more flowable ((particles below 20 µm is 0 vol%) with an AOR value of 21.33º, i.e., as expected a lower flow rate resulted in a lower AOR [18].

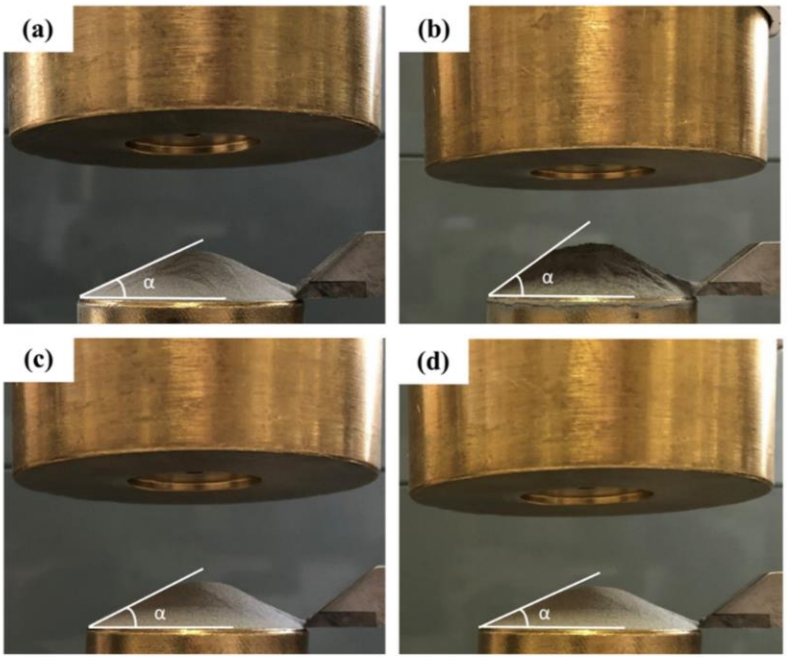

Figure 4. The angle of repose (AOR) measurements of; (a) M15-45 (22.39 º), (b) Mix1(32.85º), (c) Mix2 (22.01º), and (d) Mix3 (21.33º).

Density and flow rate results are shown in **Table 1**, and the seen flow rate of the Mix1 was not able to be quantified due to high fine powder volume. The lowest flow rate and AOR values were measured as 14.19 (s/50g) and 21.33º for Mix3, respectively. The highest apparent density measured was measured as 4.97 g cm^{-3} from Mix1, and the lowest apparent density was measured as 4.78 g cm^{-3} from Mix15-45. As could be seen the highest oxygen content was measured for Mix1 sample due probably to the higher fine power ratio making the surface area (calculated by using D50 values obtained from laser diffraction) and relatively higher than that of the others.

Table 1. Density, flow rate, AOR results (average of five consistent measurements), together with oxygen content measured by hot gas extraction, and calculated external surface area values for M15-45, Mix1, Mix2, and Mix3.

Sample Code	**M15-45**	**Mix1**	**Mix2**	**Mix3**
Apparent density [g cm^{-3}]	4.78	4.97	4.80	4.86
Tap density [g cm^{-3}]	5.29	5.55	4.96	5.23
Flow rate [s/50 g]	15.08	-	14.35	14.19
Angle of Repose [AOR, ◦]	22.39	32.85	22.01	21.33
Oxygen amount [PPM]	246	384	241	207
Calculated external surface area [m^2 g^{-1}]	0.025	0.046	0.022	0.014

3.2. Spreadability by Image Processing

Spreadability was analyzed via MATLAB on the first three spread layers. Simply; at the beginning, the raw image taken was cropped as a circle, then edge detection and threshold were applied on the cropped circle. Followed by the determination of the black to white ratio of the threshold image which was used to identify the defects on the spread layer. The obtained and processed images, and the extracted data are given in **Figure 5&6** and **Table 2,** respectively.

As seen in **Figure 5(a-c)**, no irregularity was observed from layers 1 to 3 of the spreads for M15-45. It was previously shown that M15-45 was a flowable powder (with a flow rate of 15.08 s/50 g and AOR value of 22.39^{o}) and predictably homogeneous powder layers were observed. For M15-45 powder mixture layer 1, layer 2, layer 3, average grayscale values and black to white ratios were quantified as 119.84, 115.96, 135.05, and 0.31, 0.30, 0.21, respectively.

The flow rate of Mix1 was not able to be assessed, and parallel to that clear irregularities were observed from the raw and edge detection applied images for layers 1, 2, and 3. However, these irregularities were not noticed in threshold images (see **Figure 5(d-f)**). The average grayscale values of layers 1, 2, 3 were quantified as 94.49, 91.98, 92.66, while average black to white ratios were 0.37, 0.40, 0.46. It is important to note that Mix1 was a very cohesive powder with the highest AOR (32.85^{o}) in all powder mixtures. Accordingly; different than all other samples an average grayscale value and black to the white ratio for all layers were quantified lower than 95 and higher than 0.32, respectively.

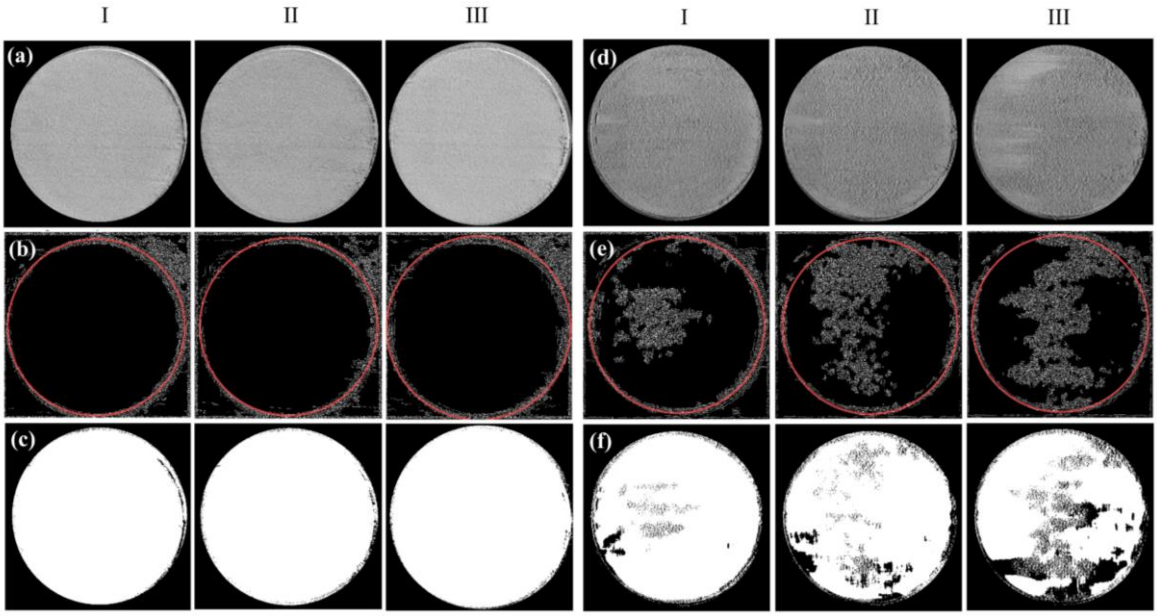

Figure 5. Cropped raw images of spread layers of M15-45 (a-I) layer 1, (a-II) layer 2, and (a-III) layer 3. The same layers after *edge detection* (b-I) layer 1, (b-II) layer 2, and (b-III) layer 3. Followed by the application of *threshold* (c-I) layer 1, (c-II) layer 2, and (c-III) layer 3. Cropped raw images of spread layers of Mix1 (d-I) layer 1, (d-II) layer 2, and (d-III) layer 3. The same layers after *edge detection* (e-I) layer 1, (e-II) layer 2, and (e-III) layer 3. Followed by the application of *threshold* (f-I) layer 1, (f-II) layer 2, and (f-III) layer 3.

Mix2 was also a flowable powder blend akin to M15-45 but the flowability was higher (with a flow rate of 14.35 s/50 g and AOR value of 22.01^{o}) due probably to coarser average particle size, compared to that of M15-45. While raw images demonstrate a homogeneous outlook (see **Figure 6(a)**), some extent of noise can be visible from the *edge detection* applied layer images (see **Figure 6(b)**) but not from the threshold applied ones given in **Figure 6(c)**. Accordingly, for Mix2 layer 1, 2, and 3, average grayscale values of 107.04, 107.38, 107.33, and black to white ratios of 0.31, 0.32, 0.31 were found, respectively.

The most flowable blend was the Mix3 with a flow rate of 14.19 s/50 g, and AOR being 21.33^{o}. High flowability caused inadequate filling in layer 1, as shown in **Figure 6(d-I)**. However, irregularities were not seen in the spread layers of 2 and 3, see **Figure 6(d-II & III)**. The average grayscale values of layers 1, 2, and 3 were quantified as 82.38, 113.67, and 115.09, while average black to white ratios were found as 0.60, 0.30, and 0.30, respectively (see **Figure 6(e&f)**).

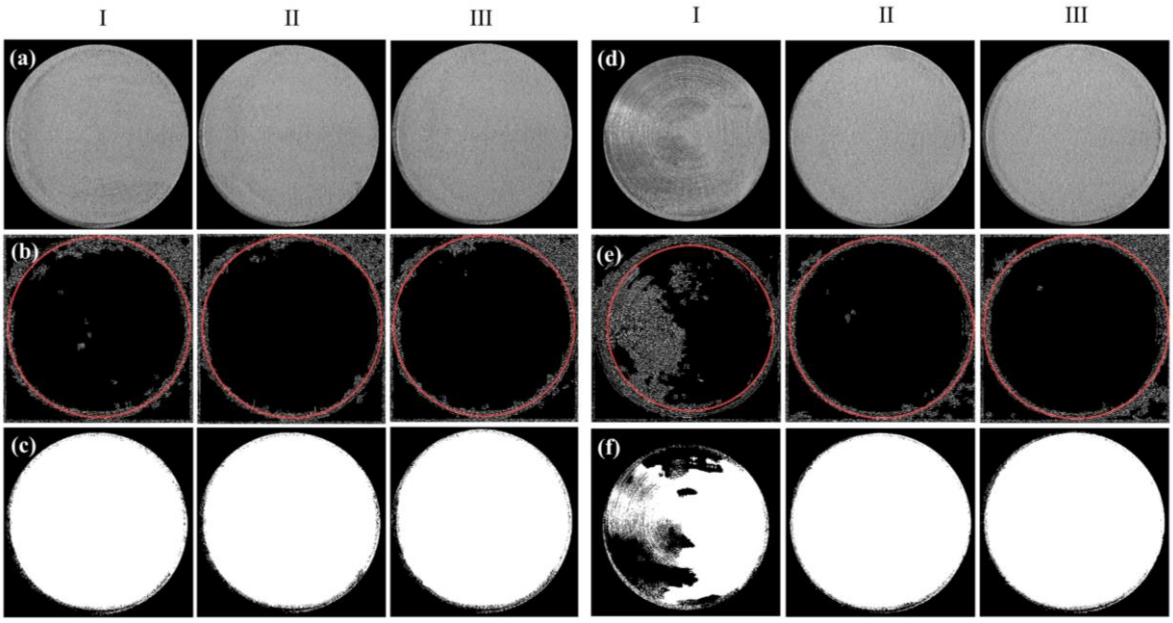

Figure 6. Cropped raw images of spread layers of Mix2 (a-I) layer 1, (a-II) layer 2, and (a-III) layer 3. The same layers after *edge detection* (b-I) layer 1, (b-II) layer 2, and (b-III) layer 3. Followed by the application of *threshold* (c-I) layer 1, (c-II) layer 2, and (c-III) layer 3. Cropped raw images of spread layers of Mix3 (d-I) layer 1, (d-II) layer 2, and (d-III) layer 3. The same layers after *edge detection* (e-I) layer 1, (e-II) layer 2, and (e-III) layer 3. Followed by the application of *threshold* (f-I) layer 1, (f-II) layer 2, and (f-III) layer 3.

Although other factors such as spreading speed, blade type highly possible to affect the spread layer characteristics [18], setting these constant while altering only the powder characteristics by changing the particle size distribution, it is possible to comment that for a homogenous layer covering, it is better to have a powder with flowability value being neither too high nor too low. Accordingly, for the tested powder blends the measured average grayscale value should not be lower than 95 on the cropped images, and black to a white ratio higher than 0.32 on threshold applied images.

Table 2. The average grayscale values (calculated from the cropped raw image) and black to white ratios (calculated from threshold image) of each layer.

Sample	**Average Grayscale Value (0 to 255)**	**Black to White Ratio**
M15-45-Layer 1	119.84	0.31
M15-45-Layer 2	115.96	0.30
M15-45-Layer 3	135.05	0.26
Mix1-Layer 1	94.49	0.37

Mix1-Layer 2	91.98	0.40
Mix1-Layer 3	92.66	0.46
Mix2-Layer 1	107.04	0.31
Mix2-Layer 2	107.38	0.32
Mix2-Layer 3	107.33	0.31
Mix3-Layer 1	82.38	0.60
Mix3-Layer 2	113.67	0.30
Mix3-Layer 3	115.09	0.30

4. Conclusions

Powder spreadability was analyzed quantitatively via image processing algorithms using MATLAB. According to the applied algorithm on the tested powder blends, average grayscale values (0 to 255) lower than 95 on cropped images, and black to a white ratio higher than 0.32 on threshold applied images, irregularities were observed. It was noted that when the powder mixture had a high flowability, it caused a reduction in the angle of repose (AOR), as seen for Mix3, demonstrating poor spreadability. In addition, when the volume fraction of fine particles (e.g., below 10 μm) increased, enhanced agglomeration decreased the flowability, and caused a similar poor spreadability effect. For example, Mix1 had the highest volume of particles sized below 10 μm (%28.06) and it demonstrated to have an average grayscale value lower than 95, and a black to a white ratio higher than 0.32. Therefore, it could be stated that when flowability is neither too high nor too low, but the one allowing an optimum coating, high-quality spreadability can be obtained. While the spread layer irregularities may cause unwanted microstructural developments, they can also be deliberately used to form porous components depending on the user's requests.

Acknowledgments

Cekdar Vakif Ahmetoglu acknowledges the support of the Alexander von Humboldt (AvH) Foundation. The authors would like to thank Ezgi Ogur, Oyku Icin, Cerem Piskin, and Esin Karatas (Department of Materials Science and Engineering, Izmir Institute of Technology) for their helps during the preparation of figures. The authors also wish to thank Dr. Kerem Altun (Department of Mechanical Engineering, Izmir Institute of Technology), Cagri Gurbuz (Sentes-BIR, Izmir, Turkey), Birhan Ufku Güzel (Laseral Endustriyel Lazer Sistemleri, Izmir, Turkey) and Firat Mavi (Mechanical Engineering, Ege University) for their support during the study.

References

[1] ISO, 2015. INTERNATIONAL STANDARD ISO/ASTM 52900: 2015 Additive manufacturing — General principles — Terminology.
[2] N. Tuncer, A. Bose, Solid-State Metal Additive Manufacturing: A Review, JOM, 72 (2020) 3090-3111.
[3] C.N. Kuo, C.K. Chua, P.C. Peng, Y.W. Chen, S.L. Sing, S. Huang, Y.L. Su, Microstructure evolution and mechanical property response via 3D printing parameter development of Al–Sc alloy, Virtual and Physical Prototyping, 15 (2020) 120-129.
[4] J. Bi, Z. Lei, Y. Chen, X. Chen, Z. Tian, J. Liang, X. Qin, X. Zhang, Densification, microstructure and mechanical properties of an Al-14.1Mg-0.47Si-0.31Sc-0.17Zr alloy printed by selective laser melting, Materials Science and Engineering: A, 774 (2020) 138931.
[5] S. Wen, C. Wang, Y. Zhou, L. Duan, Q. Wei, S. Yang, Y. Shi, High-density tungsten fabricated by selective laser melting: Densification, microstructure, mechanical and thermal performance, Optics & Laser Technology, 116 (2019) 128-138.
[6] Z. Du, H.-C. Chen, M.J. Tan, G. Bi, C.K. Chua, Effect of nAl2O3 on the part density and microstructure during the laser-based powder bed fusion of AlSi10Mg composite, Rapid Prototyping Journal, 26 (2020) 727-735.
[7] R. Martinez, I. Todd, K. Mumtaz, In situ alloying of elemental Al-Cu12 feedstock using selective laser melting, Virtual and Physical Prototyping, 14 (2019) 242-252.
[8] S. Huang, S.L. Sing, G. de Looze, R. Wilson, W.Y. Yeong, Laser powder bed fusion of titanium-tantalum alloys: Compositions and designs for biomedical applications, Journal of the Mechanical Behavior of Biomedical Materials, 108 (2020) 103775.
[9] W. Zhang, A. Mehta, P.S. Desai, C. Higgs, Machine learning enabled powder spreading process map for metal additive manufacturing (AM), Int. Solid Free Form Fabr. Symp. Austin, TX, 2017, pp. 1235-1249.
[10] L. Cordova, T. Bor, M. de Smit, M. Campos, T. Tinga, Measuring the spreadability of pre-treated and moisturized powders for laser powder bed fusion, Additive Manufacturing, 32 (2020) 101082.
[11] S. Vock, B. Klöden, A. Kirchner, T. Weißgärber, B. Kieback, Powders for powder bed fusion: a review, Progress in Additive Manufacturing, 4 (2019) 383-397.
[12] ISO, 2019. INTERNATIONAL STANDARD ISO /ASTM 52907: 2019 Additive manufacturing — Feedstock materials — Methods to characterize metallic powders.
[13] A. Mussatto, R. Groarke, A. O'Neill, M.A. Obeidi, Y. Delaure, D. Brabazon, Influences of powder morphology and spreading parameters on the powder bed topography uniformity in powder bed fusion metal additive manufacturing, Additive Manufacturing, 38 (2021) 101807.
[14] H. Gu, H. Gong, J. Dilip, D. Pal, A. Hicks, H. Doak, B. Stucker, Effects of powder variation on the microstructure and tensile strength of Ti6Al4V parts fabricated by selective laser melting, Proceedings of the 25th annual international solid freeform fabrication symposium, austin, tx, usa, 2014, pp. 4-6.
[15] M. Balbaa, A. Ghasemi, E. Fereiduni, M. Elbestawi, S. Jadhav, J.-P. Kruth, Role of powder particle size on laser powder bed fusion processability of AlSi10mg alloy, Additive Manufacturing, 37 (2021) 101630.
[16] M.J. Heiden, L.A. Deibler, J.M. Rodelas, J.R. Koepke, D.J. Tung, D.J. Saiz, B.H. Jared, Evolution of 316L stainless steel feedstock due to laser powder bed fusion process, Additive Manufacturing, 25 (2019) 84-103.
[17] D. Geldart, E.C. Abdullah, A. Hassanpour, L.C. Nwoke, I. Wouters, Characterization of powder flowability using measurement of angle of repose, China Particuology, 4 (2006) 104-107.

[18] Z. Snow, R. Martukanitz, S. Joshi, On the development of powder spreadability metrics and feedstock requirements for powder bed fusion additive manufacturing, Additive Manufacturing, 28 (2019) 78-86.
[19] A.T. Sutton, C.S. Kriewall, S. Karnati, M.C. Leu, J.W. Newkirk, Characterization of AISI 304L stainless steel powder recycled in the laser powder-bed fusion process, Additive Manufacturing, 32 (2020) 100981.
[20] D. Powell, A.E.W. Rennie, L. Geekie, N. Burns, Understanding powder degradation in metal additive manufacturing to allow the upcycling of recycled powders, Journal of Cleaner Production, 268 (2020) 122077.
[21] L. Brandon, W. Eric, M. Shawn, Multiple sensor detection of process phenomena in laser powder bed fusion, Proc.SPIE, 2016.
[22] J.K. Prescott, R.A. Barnum, On powder flowability, Pharmaceutical technology, 24 (2000) 60-85.
[23] S.E. Brika, M. Letenneur, C.A. Dion, V. Brailovski, Influence of particle morphology and size distribution on the powder flowability and laser powder bed fusion manufacturability of Ti-6Al-4V alloy, Additive Manufacturing, 31 (2020) 100929.
[24] L.I. Escano, N.D. Parab, L. Xiong, Q. Guo, C. Zhao, K. Fezzaa, W. Everhart, T. Sun, L. Chen, Revealing particle-scale powder spreading dynamics in powder-bed-based additive manufacturing process by high-speed x-ray imaging, Scientific reports, 8 (2018) 1-11.
[25] H. Chen, Q. Wei, Y. Zhang, F. Chen, Y. Shi, W. Yan, Powder-spreading mechanisms in powder-bed-based additive manufacturing: Experiments and computational modeling, Acta Materialia, 179 (2019) 158-171.
[26] W. Nan, M. Pasha, T. Bonakdar, A. Lopez, U. Zafar, S. Nadimi, M. Ghadiri, Jamming during particle spreading in additive manufacturing, Powder Technology, 338 (2018) 253-262.
[27] C. Meier, R. Weissbach, J. Weinberg, W.A. Wall, A. John Hart, Modeling and characterization of cohesion in fine metal powders with a focus on additive manufacturing process simulations, Powder Technology, 343 (2019) 855-866.
[28] M. Ahmed, M. Pasha, W. Nan, M. Ghadiri, A simple method for assessing powder spreadability for additive manufacturing, Powder Technology, 367 (2020) 671-679.
[29] ASTM-American Society for Testing and Materials, 2015a. ASTM D3576-15 Standard Test Method for Cell Size of Rigid Cellular Plastics, ASTM International, West Conshohocken, PA.
[30] T. Semerci, M.D. de Mello Innocentini, G.A. Marsola, P.R.O. Lasso, G.D. Soraru, C. Vakifahmetoglu, Hot Air Permeable Preceramic Polymer Derived Reticulated Ceramic Foams, ACS Applied Polymer Materials, 2 (2020) 4118-4126.
[31] A. Bootz, V. Vogel, D. Schubert, J. Kreuter, Comparison of scanning electron microscopy, dynamic light scattering and analytical ultracentrifugation for the sizing of poly(butyl cyanoacrylate) nanoparticles, European Journal of Pharmaceutics and Biopharmaceutics, 57 (2004) 369-375.